

Changes in Regional Ventilation after Autologous Blood Clot Pulmonary Embolism

Marcos F. Vidal Melo, M.D., Ph.D.,* R. Scott Harris, M.D.,† Dominick Layfield, B.S.,‡ Guido Musch, M.D.,* Jose G. Venegas, Ph.D.§

Background: Previous studies have suggested that pulmonary embolism (PE) and pulmonary artery occlusion result in a shift in alveolar ventilation away from unperfused regions. This study aimed to directly assess changes in regional specific ventilation (\dot{V}_A) due to autologous blood clot PE using positron emission tomography.

Methods: Pulmonary embolism was created in six anesthetized, paralyzed, and mechanically ventilated sheep by injecting cylindrical clots of autologous blood (7 mm in diameter and height). Clots were progressively infused into a central vein until a stable mean pulmonary artery pressure between 30 and 40 mmHg was achieved. A multislice positron emission tomography camera was used to image 15 contiguous, 6.5-mm-thick transverse cross-sections of the chest beginning just above the diaphragm. \dot{V}_A from perfused regions ($\dot{V}_{A,p}$) was assessed as the ventilatory turnover rate of the tracer ^{13}NN after central venous injection of ^{13}NN -labeled saline.

Results: Pulmonary embolism obstructed flow to 64% of imaged areas. Before PE, $\dot{V}_{A,p}$ was equivalent in areas that would remain perfused and those that would become embolized after PE (0.021 ± 0.007 vs. 0.021 ± 0.006 s^{-1} ; $P = \text{nonsignificant}$). After PE, $\dot{V}_{A,p}$ of areas remaining perfused increased to 0.033 ± 0.011 s^{-1} ($P < 0.005$). This effect on regional $\dot{V}_{A,p}$ could have been caused by active redistribution of $\dot{V}_{A,p}$ or by a reduction in tracer concentration of perfused areas due to the dead space common to perfused and embolized regions. Model simulations indicated that the common dead-space effect could only explain a small part of the $\dot{V}_{A,p}$ increase.

Conclusions: An increase in \dot{V}_A of perfused regions occurs following PE with 7-mm autologous blood clots. This increase is most likely caused by a shift in ventilation away from embolized areas mediated by hypocapnic pneumoconstriction.

A SHIFT in ventilation away from unperfused lung regions has been demonstrated following pulmonary artery occlusion (PAO).^{1,2} This shift was described as early as 1934, when Moore *et al.*³ reported that ligation of either the left or right pulmonary artery resulted in a reduction of ventilation to the unperfused lung with an increase in ventilation of the perfused lung. Severing-

haus *et al.*² showed that temporary unilateral PAO in dogs resulted in a shift of ventilation away from the unperfused lung caused by regional bronchoconstriction and that the shift was prevented by inhalation of 6% CO_2 . This study pointed to the concept of hypocapnic bronchoconstriction as a homeostatic mechanism leading to compensation of the ventilation-perfusion (\dot{V}_A/\dot{Q}) mismatch caused by pulmonary embolism (PE). Subsequent investigations showed mechanical changes also at the lung tissue level during PAO and PE,^{1,4,5} and the broader term *pneumoconstriction* was adopted to characterize the activation of contractile elements related to the connective matrix structure.

Acute PE in the clinical setting frequently leads to important gas exchange abnormalities. If a ventilatory shift away from embolized regions were present in such conditions, it would tend to reduce the impairment in gas exchange. However, the existence and quantification of a shift in ventilation away from embolized regions during pulmonary thromboembolism is not completely established. Thomas *et al.*⁶ demonstrated that airway resistance increases following embolization of autologous thrombi to dog lungs. Levy and Simmons⁷ used computations of regional ventilation based on postmortem examination of dog lungs embolized with autologous thrombi to indirectly suggest that regional pulmonary hypoperfusion at a lobar and segmental level resulted in changes in effective alveolar ventilation compatible with a shift of ventilation from embolized to perfused regions. However, direct measurements of regional ventilation changes with PE caused by autologous blood clots have not been performed.

We measured changes in regional lung expansion and gas tracer washout after unilateral PAO in dogs using planar positron imaging of the washout of equilibrated ^{13}NN gas. These measurements suggested that increased regional lung impedance shifted ventilation toward the perfused lung at normal breathing frequencies because of mechanical constriction at the tissue level in the unperfused lung.¹ That imaging method has been adapted to three-dimensional assessment of regional ventilation and perfusion with positron emission tomography (PET).⁸

In the current study, we used this technique to investigate changes in regional ventilation following acute and severe PE induced by infusion of autologous blood clots of precise size. We theorized that if minute ventilation was kept constant, regional ventilation would increase in the areas that remained perfused after PE as a result of a redistribution of tidal volume away from embolized areas.

* Instructor of Anesthesia, Harvard Medical School, Assistant Anesthetist, Massachusetts General Hospital. † Instructor in Medicine, Harvard Medical School, Assistant in Medicine, Massachusetts General Hospital. ‡ Graduate Student, Massachusetts Institute of Technology, Cambridge, Massachusetts. § Associate Professor of Anesthesia (Bioengineering), Harvard Medical School and Massachusetts General Hospital.

Received from the Department of Anesthesia and Critical Care, Massachusetts General Hospital and Harvard Medical School, Boston, Massachusetts. Submitted for publication November 14, 2001. Accepted for publication April 2, 2002. Supported by grant No. HL-38267 from the National Heart, Lung, and Blood Institute, Bethesda, Maryland. Presented in part at the annual meetings of the American Thoracic Society, San Francisco, California, May 23, 2001, and the American Society of Anesthesiologists, New Orleans, Louisiana, October 15, 2001.

Address reprint requests to Dr. Vidal Melo: Cardiac Anesthesia Group, Department of Anesthesia and Critical Care, Massachusetts General Hospital, 55 Fruit Street, Boston, Massachusetts 02114. Address electronic mail to: mvidalmelo@partners.org. Individual article reprints may be purchased through the Journal Web site, www.anesthesiology.org.

Methods

The experimental protocol was approved by the Massachusetts General Hospital Committee on Animal Care.

Experimental Apparatus

The apparatus included a PET camera, a mechanical ventilator coupled with two breathing circuits, and a tracer infusion system. The PET camera was a multiring full-body camera (Scanditronix PC4096; General Electric, Milwaukee, WI) with detectors positioned around circular rings. The breathing system was designed to allow for volume-controlled ventilation with fresh gas or with tracer containing gas from a closed circuit. The closed breathing circuit included a carbon dioxide absorber and a servo-controlled supplemental oxygen source to replace metabolic oxygen consumption and maintain a constant circuit volume. Remotely controlled solenoid valves allowed instantaneous switching between the two breathing circuits. The closed circuit was used for equilibration of the air spaces with ^{13}NN before washout maneuvers. This system kept a constant breathing pattern irrespective of the circuit being used, and it had low internal volume to minimize dilution of the ^{13}NN tracer and allow for faster gas equilibration. The infusion system consisted of a computer-controlled device for production and injection of the ^{13}NN -saline solution. The tracer ^{13}NN gas (~ 10 -min half-life) was generated by a cyclotron and dissolved in degassed saline, yielding a specific activity that ranged from 0.22 to 0.65 mCi/ml. A rapid bolus of ^{13}NN -labeled saline (10–30 ml) was injected into a central vein at a rate of 10 ml/s under computer control.

Animal Preparation

Six sheep weighing 17 kg (range, 14–19 kg) were anesthetized, intubated, and mechanically ventilated while in the prone position. General anesthesia was induced with an intravenous bolus of sodium thiopental (35 mg/kg) and maintained with a continuous infusion of sodium thiopental ($15 \text{ mg} \cdot \text{kg}^{-1} \cdot \text{h}^{-1}$). Pancuronium (0.2 mg/kg) was used for muscle paralysis. The ventilator (Harvard Apparatus, Millis, MA) was set at an inspired oxygen fraction (FiO_2) of 1.0, positive end-expiratory pressure of 5 cm H_2O , tidal volume (V_T) of 17 ml/kg (285 ± 41 ml), and inspiratory time of 30% of the breathing period. Respiratory rate (14 ± 4 breaths/min) was set to maintain normocapnic arterial blood gases at the beginning of the experiment and fixed at that value for the rest of the experiment. The right femoral artery was cannulated for systemic arterial pressure monitoring and blood sampling and the right femoral vein for administration of drugs. A Swan-Ganz catheter (model 93A-131H-7F; Edwards Laboratory, Santa Ana, CA) was inserted in the left femoral vein and advanced into the pulmonary artery. Its distal port was used for monitoring

of pulmonary arterial pressure (PAP) and sampling of pulmonary arterial blood. A central line was introduced in a jugular vein and positioned into the superior vena cava for delivery of the ^{13}NN -labeled saline solution. A second and larger (7-mm ID) central line was introduced into the contralateral internal jugular vein and used for infusion of the autologous blood clots.

Production of Blood Clots and Induction of Pulmonary Embolism

Autologous clots were produced in cylindrical molds of equal height and diameter (9 mm) drilled on a board of Plexiglas. At the beginning of the animal preparation, 150 ml of blood was drawn from the animal and left to clot in the Plexiglas molds. Blood loss was substituted by simultaneous infusion of 450 ml of normal saline to account for distribution of crystalloid in extracellular fluid. Approximately 1 h after clotting of the blood, a rod was used to extrude the clots. Final dimensions of the clots, after clot retraction, were approximately 7-mm diameter and 7-mm height. PE was induced by progressive infusion of individual clots (average of 24; range, 13–33) until a stable mean PAP in the range of 30–40 mmHg was maintained for 1 h. Administration of crystalloids (500–1,500 ml) was used to prevent a decrease in mean arterial blood pressure to less than 50 mmHg during and after the induction of PE.

Imaging Protocol

The animal was positioned in the camera field with the most caudal slice adjacent to the diaphragm dome. The PET camera collected 15 transverse cross-sectional slices of 6.5-mm thickness providing three-dimensional information over a 9.7-cm-long cylinder. We estimate that the imaged lung corresponded to approximately 85% of the total lung volume. Transmission scans were obtained before each set of emission scans to correct for absorption of annihilation photons in the animal's body. For this, a radioactive source was rotated around the imaging field and the resulting signal used for reconstruction of an image that can be compared with a low-resolution computed tomography scan. Regional density was inferred from this image as the amount of the initial radioactive beam absorbed by the tissues at each point in the animal's body. Emission scans of local tracer activity were reconstructed with appropriate correction for detector sensitivity and for tissue attenuation using a convolution back-projection algorithm with a Hanning filter yielding an effective in-plane resolution of 6 mm (determined from the width at one-half height of a point source image). Resulting images consisted of an interpolated matrix of $128 \times 128 \times 15$ voxels of $6 \times 6 \times 6.5$ mm. Images were then lowpass filtered to a spatial resolution of $12 \times 12 \times 6.5$ mm to minimize imaging noise. These filtered raw images were processed following the methodology described in the sections Regional

Perfusion, Regional Ventilation, and Regional Gas Volume to yield functional images.

Imaging protocol for the emission scans was conducted as follows: starting with a tracer-free lung, the ventilator was turned off at end exhalation, and a bolus of ^{13}NN saline solution (~ 9 mCi) was injected into a central vein. Simultaneously, collection of six consecutive scans of 5-s duration was started while the animal was kept in apnea for 30 s. At the end of these scans, mechanical ventilation was resumed, and the lungs were imaged as the tracer washed out of the lungs. The washout serial scans consisted of four scans of 30-s duration and two scans of 60-s duration for a total of 240 s of imaging time. A sample of the infusate was collected to assess its specific activity in a well counter cross-calibrated with the PET camera.

An additional protocol was introduced in the last three experiments to assess ventilation from embolized regions of interest (ROIs). The experimental protocol consisted of ventilating the lungs with a closed breathing circuit containing ^{13}NN -labeled gas. A sequence of images was obtained during this wash-in equilibration phase. After 4 min, ventilation was stopped at end expiration, and the lungs were imaged for 30 s. The inspiratory gas was then switched to label-free gas, ventilation was restarted, and a sequence of images as described in the previous paragraph was collected as the tracer washed out from the lungs. A 1-ml gas sample was obtained from the rebreathing circuit to assess its specific activity in the cross-calibrated well counter.

Regional Perfusion

The method to generate images of regional perfusion (\dot{Q}_r) was based on the extremely low solubility of nitrogen (partition coefficient = 0.018) in blood and tissues. Due to this property, following an intravenous injection of ^{13}NN -saline solution, virtually all the ^{13}NN tracer gas in the blood diffuses into alveolar gas spaces at the first pass in normal and aerated lung units. If the lungs are kept apneic during and after tracer arrival, tracer content, and thus local radioactivity, in these aerated units remains nearly constant and is therefore proportional to \dot{Q}_r . The image of \dot{Q}_r was computed as the average of the scans taking place during the plateau phase of apnea normalized by the mean tracer concentration over the imaged lung.

Selection of Voxels for Analysis

Initial masks for the lung fields before and after PE were created by thresholding the respective transmission scans to areas with density less than 50% of the mean tissue density. Subsequently, the perfusion image after PE was used to define ROIs for "perfused" and "embolized" areas. The ROI for perfused areas was obtained by automatically thresholding the corresponding perfusion image to a level that included 85% of imaged

lung perfusion. For this, voxels were sorted by their perfusion and, starting from the voxel with the highest perfusion, additional voxels were included in the image until 85% of the total perfusion was reached. Voxels in the lung field not included in the perfused ROI formed the embolized ROI, *i.e.*, these areas accounted for only 15% of total lung perfusion. In the cases where a tracer equilibration image was available, this image was used in place of the transmission scans to generate the lung field masks.

Regional Ventilation

Tracer kinetics within perfused and embolized ROIs were obtained from the washout serial scans by plotting average tracer activity measured for each scan *versus* time. Time corresponding to each scan was set at the middle of the respective scanning period. From these plots, we estimated local specific ventilation (ventilation per unit of gas volume, \dot{V}_A) in terms of the washout turnover rate of ^{13}NN in two conditions: following apneic intravenous bolus injection of ^{13}NN saline ($\dot{V}_{A,p}$) and following equilibration of inhaled ^{13}NN ($\dot{V}_{A,i}$). $\dot{V}_{A,p}$ and $\dot{V}_{A,i}$ were estimated from the average turnover rate from the first to the second 30-s scan of the washout phase. This was based on the fact that, for a multicompartmental system, the turnover rate at the beginning of the washout corresponds to the average of the turnover rates weighted by perfusion ($\dot{V}_{A,p}$) or volume ($\dot{V}_{A,i}$).

The $\dot{V}_{A,p}$ could not be calculated after embolism for the embolized ROIs because of absence of injected tracer in these regions. To assess ventilation from these regions, in the last three experiments, the washout rate of ^{13}NN -labeled gas previously equilibrated in lungs $\dot{V}_{A,i}$ was calculated.⁹ $\dot{V}_{A,i}$ was computed from the sequence of images during washout with the same algorithm as for $\dot{V}_{A,p}$.

The $\dot{V}_{A,p}$ and $\dot{V}_{A,i}$ were calculated for the perfused and embolized ROIs before and after PE. These variables were computed on a voxel-by-voxel basis to calculate spatial heterogeneity, spatial correlation, and fractional distribution.

Regional Gas Volume

Regional gas volume (V_p) was calculated in the last three experiments from equilibration images of inhaled ^{13}NN . Because of the low solubility of nitrogen in body fluids and tissues, at the end of the wash-in equilibration period, ^{13}NN was mostly confined to air spaces within the lungs. Thus, after equilibration, the tracer concentration in the lungs was proportional to the regional gas content. The alveolar gas content per voxel image (V_p) was obtained by normalizing voxel activity values by the specific activity of the equilibrated gas, after correction for radioactive decay. With the calculated regional gas volume, mean-normalized absolute ventilation of per-

fused tracer ($\dot{V}_{A,p}$) was computed as the product of $s\dot{V}_{A,p}$ and the regional gas content.

Spatial Heterogeneity

The spatial heterogeneity of the functional images of $s\dot{V}_{A,p}$ and \dot{Q}_r was assessed from the coefficient of variation of the voxel data defined as the SD normalized by the mean value of the data: coefficient of variation = SD/mean within the lung field.

Spatial Correlations

The spatial correlation coefficient between two regional variables was calculated from the Pearson coefficient of corresponding functional images on a voxel-by-voxel basis. Spatial correlation was calculated for the following pairs of variables: V_r , \dot{Q}_r , and $\dot{V}_{A,p}$ before and after embolism and for V_r versus \dot{Q}_r , $\dot{V}_{A,p}$ versus \dot{Q}_r , and $s\dot{V}_{A,p}$ versus $s\dot{V}_{A,i}$ in control and PE conditions.

Fractional Distributions

The $s\dot{V}_{A,p}$ was computed in each voxel for perfused ROIs before and after PE and used to generate frequency distribution histograms. The distributions were characterized by the corresponding mean, SD, and coefficient of variation.

Physiologic Measurements

In addition to PET data, the following variables were measured: (1) cardiovascular: heart rate, invasive systemic blood pressure, PAP, PAO pressure, and cardiac output; (2) respiratory: V_T , respiratory rate, FiO_2 , peak airway pressure, arterial and mixed venous blood gases, right-to-left shunt, venous admixture, end-tidal carbon dioxide partial pressure (P_{ETCO_2}), mixed-expired P_{CO_2} , and Bohr dead space (V_D/V_T). Mixed-expired P_{CO_2} was assessed by measuring P_{CO_2} concentration with an infrared analyzer in a mixing chamber placed in the expiratory limb of the breathing system. The usual equation $V_D/V_T = (P_{aCO_2} - P_{E CO_2})/P_{aCO_2}$ was used to calculate Bohr dead space.

Statistical Analysis

Comparisons between control and PE were made using the two-tailed Student *t* test for paired samples. Data were expressed as mean \pm SD. Pearson correlation coefficient (*r*) was calculated to study the agreement between $s\dot{V}_{A,p}$ and $s\dot{V}_{A,i}$. Spearman correlation was used to summarize the relation between the change in $s\dot{V}_{A,p}$ from before to after PE in perfused areas and arterial pH. This method reduces the influence of outliers in the computation of the correlation coefficient. Statistical significance was taken at $P < 0.05$.

Results

Pulmonary autologous embolization resulted in marked changes in perfusion distribution. Embolized

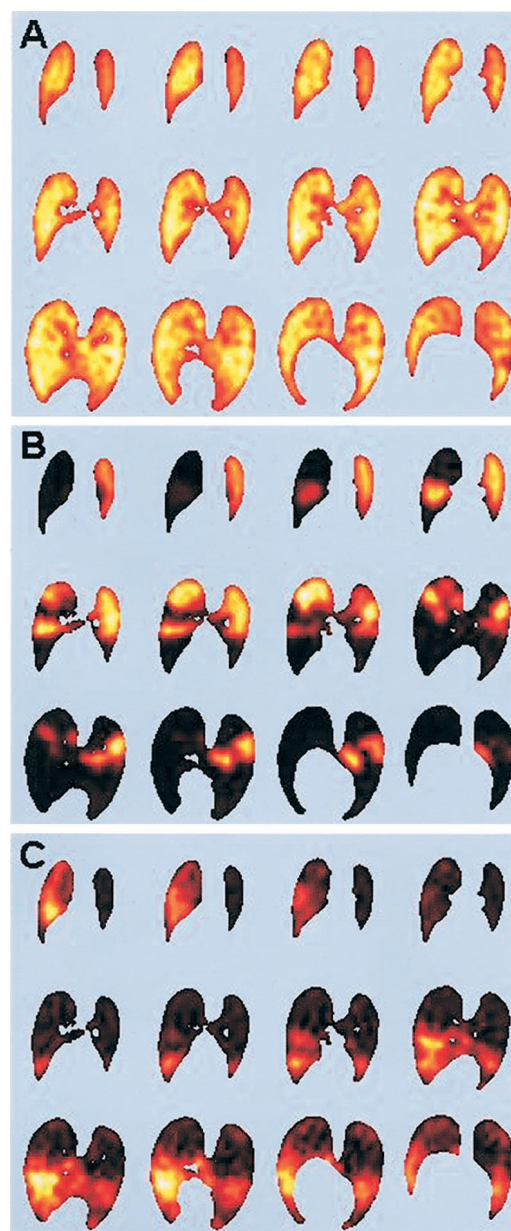


Fig. 1. Functional lung images in one animal. Images are contiguous tomographic sections viewed in the cranio-caudal direction and presented from top left to bottom right. The left side in the image corresponds to left side in the animal. Tracer activity is represented in a "hot" color scale (black = no activity; white = maximal activity) in that frame. (A) Regional perfusion (\dot{Q}_r) before embolism. (B) \dot{Q}_r after embolism. There is dramatic redistribution of \dot{Q}_r with many regions of the lungs essentially unperfused. (C) Tracer activity remaining in the lungs at the end of the washout period after inhalational delivery of tracer. Note that higher activity corresponds to embolized areas, representing the slower washout rate of these regions.

areas corresponded to $64 \pm 12\%$ of the total perfusion in the imaged areas before PE (fig. 1).

Changes in physiologic variables caused by pulmonary embolization are summarized in table 1. Significant pulmonary hypertension was achieved in this animal model with an average 2.4-fold increase in mean PAP. Changes in arterial blood gases indicated a severe respiratory

Table 1. Physiologic Measurements before and after Induction of Pulmonary Embolism

	Control	PE	P
HR (beats/min)	110 ± 22	114 ± 25	NS
MBP (mmHg)	88 ± 12	75 ± 13	NS
CO (l/min)	2.8 ± 0.7	3.9 ± 1.3	0.05
MPAP (mmHg)	14 ± 3	32 ± 3	0.001
PAOP (mmHg)	3 ± 2	10 ± 4	0.005
P _{peak} (cm H ₂ O)	24 ± 6	31 ± 6	0.005
pH	7.43 ± 0.06	7.21 ± 0.09	0.001
P _{CO₂} (mmHg)	36 ± 4	57 ± 10	0.001
P _{O₂} (mmHg)	512 ± 38	495 ± 40	NS
V _D /V _T	0.56 ± 0.12	0.80 ± 0.05	0.002

HR = heart rate; MBP = mean blood pressure; CO = cardiac output; MPAP = mean pulmonary artery pressure; PAOP = pulmonary artery occlusion pressure; P_{peak} = peak airway pressure; P_{CO₂} = partial pressure of carbon dioxide; P_{O₂} = partial pressure of oxygen; V_D/V_T = dead space ventilation.

acidosis secondary to a markedly increased V_D/V_T. P_{aO₂} did not change significantly with PE despite the severity of the embolization produced. Peak airway pressures increased 29% after PE. Cardiac output and PAO pressure were also increased after embolization.

Tracer Kinetics

Tracer kinetics in perfused and embolized ROIs after intravenous injection of ¹³NN before and after PE are shown in figure 2. As expected for a normal lung, the tracer kinetics during control conditions were essentially equivalent for regions that would become embolized or remained perfused after PE. Mean sV̇_{A,P} before embolism was 0.021 ± 0.006 s⁻¹ for regions that would become

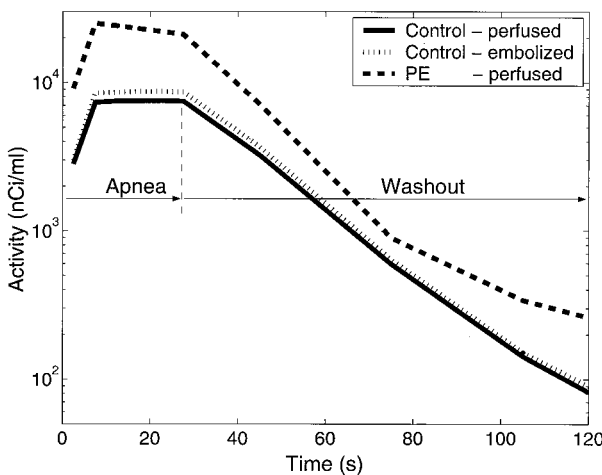


Fig. 2. Semilog plot of tracer activity versus time following central venous injection of ¹³NN during control conditions and after induction of pulmonary embolism in a typical experiment. For control conditions, curves are shown separately for perfused (continuous line) and embolized (dotted line) regions of interest (ROIs). The dashed line represents tracer kinetics for the perfused ROIs after induction of pulmonary embolism. Note the increase in turnover rate (slope) at the beginning of the washout phase compared with the same region during control conditions. Activity during the apneic phase (initial plateaus for each curve) is higher after pulmonary embolism because these areas received 85% of the injected tracer.

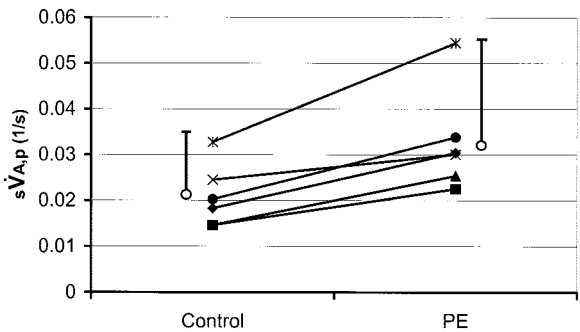


Fig. 3. Specific ventilation in regions that would remain perfused after pulmonary embolism (PE) measured with intravenous injection of ¹³NN (sV̇_{A,P}) before (control) and after PE for the six experiments. Mean sV̇_{A,P} values ± SD are shown as open circles.

embolized ROIs and 0.021 ± 0.007 s⁻¹ for regions that remained perfused after PE.

After PE there was a significant increase in the washout rate of injected tracer from regions that remained perfused (fig. 2). On average, sV̇_{A,P} increased from 0.021 ± 0.007 s⁻¹ to 0.033 ± 0.011 s⁻¹ (*P* < 0.005; fig. 3). Of interest, in the population of studied sheep, changes in sV̇_{A,P} caused by PE correlated with arterial pH measured after PE (*r* = 0.89; *P* < 0.05), *i.e.*, the lower the pH after pE, the lesser the change caused in sV̇_{A,P} by PE.

Results from the three experiments with inhaled tracer were consistent with those from injected tracer. As expected for a normal lung, no difference was observed in sV̇_{A,i} of perfused (0.025 ± 0.008 s⁻¹) and embolized (0.025 ± 0.009 s⁻¹) ROIs in control conditions (fig. 4A). After embolization, higher sV̇_{A,i} was observed in the perfused ROIs (0.028 ± 0.012 s⁻¹) as compared with the embolized ROIs (0.019 ± 0.007 s⁻¹) and to the perfused ROIs before PE. A change in the tracer washout pattern was also observed in these experiments with strongly nonlinearities obtained after PE (fig. 4B). Even though the sample size was small, measurements of sV̇_{A,P} and sV̇_{A,i} tended to correlate in the perfused ROIs before (*r* = 0.99; *P* < 0.05) and after (*r* = 0.98; *P* < 0.1) PE, with values of sV̇_{A,P} larger than sV̇_{A,i} (mean, 0.006; range, 0–0.013; *P* < 0.12).

Histograms representing frequency distribution of sV̇_{A,P} in voxels within perfused ROIs after embolism showed a shift of the mean sV̇_{A,P} to the right as compared with control conditions corresponding to a faster tracer washout in the perfused ROIs after embolization (fig. 5). Interestingly, the coefficient of variation of sV̇_{A,P} for voxels within these ROIs was reduced from 0.33 ± 0.10 during control conditions to 0.21 ± 0.04 after PE (*P* < 0.01).

There were marked changes in V_r, Q̇_r, and sV̇_{A,P} from before to after PE. Spatial correlations between control and post-PE values were 0.45 ± 0.14 (*P* < 0.001) for V_r, 0.16 ± 0.21 for Q̇_r, and 0.02 ± 0.06 for sV̇_{A,P}. Analysis of

Downloaded from http://asas.silverchair.com/anesthesiology/article-pdf/97/3/671/336570/000542-200209000-00022.pdf by guest on 10 April 2024

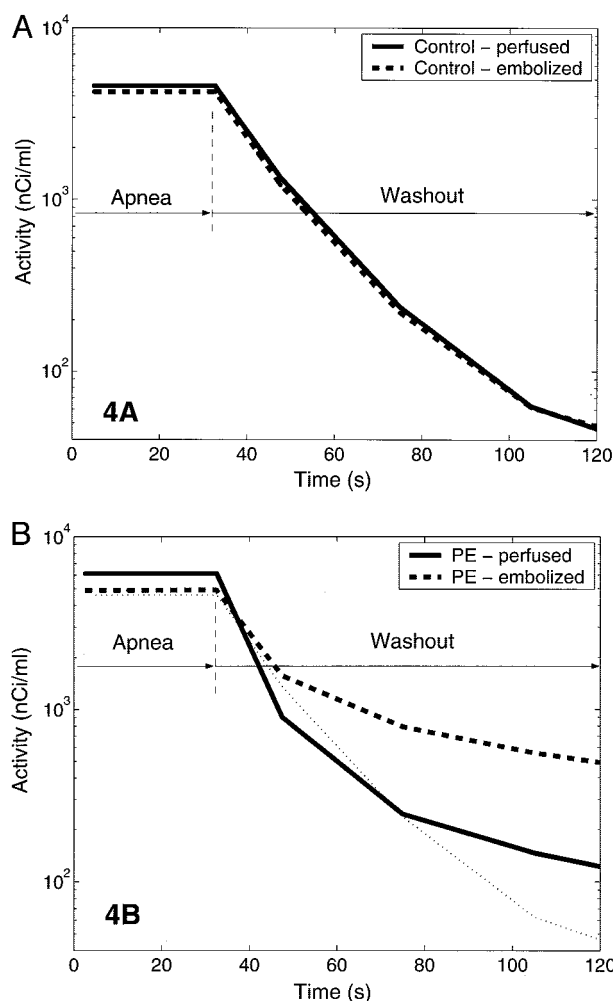


Fig. 4. Semilog plot of tracer activity *versus* time following inhalational delivery of tracer during (A) control conditions and (B) after pulmonary embolism (PE). For each condition, curves are shown separately for perfused and embolized regions of interest (ROIs). (A) During control conditions, tracer washouts are linear and equivalent in regions that would become perfused and embolized after PE. (B) After PE, the curve for perfused ROIs shows an increased slope at the beginning of the washout phase as compared with the same regions during control conditions (dotted line). Tracer washout from embolized ROIs is reduced as compared with the same regions before PE and also to the regions that remained perfused after PE. Evident nonlinearity is observed in both perfused and embolized ROIs.

the bivariate distribution of regional perfusion before and after PE showed that voxels receiving very low \dot{Q}_r after PE had a wide range of \dot{Q}_r values before embolism (fig. 6). Projections of the frequency distribution of relative perfusion before and after PE evidence the change in perfusion distribution from an approximately normal distribution to a bimodal pattern. A large peak of very low to zero perfusion (embolized areas) and a second maximum at mean-normalized perfusion values after PE around 2, representing regions that remained perfused after PE, can be observed. Spatial correlation of V_r *versus* \dot{Q}_r was substantially reduced from 0.53 ± 0.03 to $0.14 \pm$

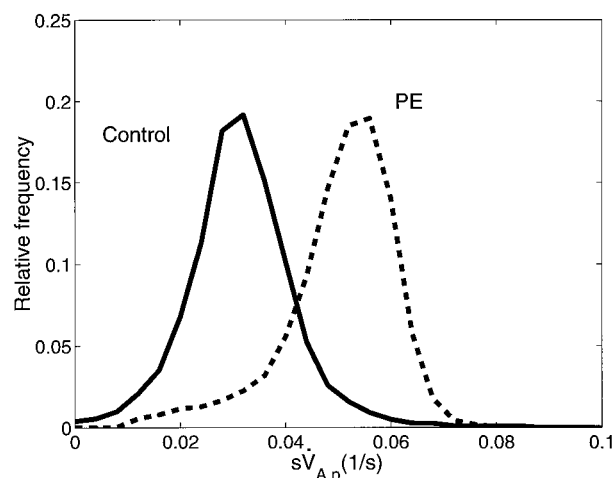


Fig. 5. Histograms of specific ventilation after injected tracer ($s\dot{V}_{A,p}$) for each image voxel in the perfused regions of interest computed for a typical experiment before (continuous line) and after (dotted line) pulmonary embolism (PE). The number of regions with high specific ventilation is increased after PE corresponding to a shift of ventilation to perfused regions.

0.20 ($P < 0.05$) after PE. Spatial correlation between $\dot{V}_{A,p}$ and \dot{Q}_r also decreased with PE from 0.34 ± 0.14 to 0.15 ± 0.11 ($P < 0.10$). Spatial correlations between $s\dot{V}_{A,p}$ and $s\dot{V}_{A,i}$ for the three experiments with inhaled tracer were 0.16 ± 0.03 for the whole lung before PE. For the perfused areas, spatial correlations changed from 0.12 ± 0.04 during control conditions to 0.07 ± 0.05 after PE.

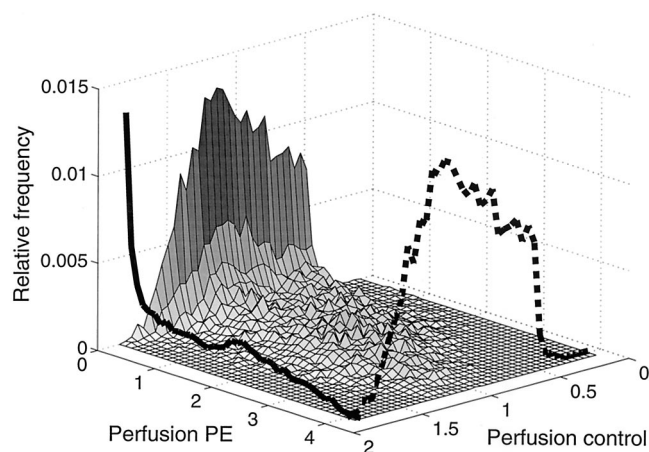


Fig. 6. Bivariate distribution of mean normalized regional perfusion for a typical animal. Height of surface over the x-y plane in the surface plot represents the fraction of voxels containing the respective combination of mean normalized regional perfusion before (control) and after pulmonary embolism (PE). Note the large number of regions with very low perfusion after PE corresponding to a wide range of regional perfusion values before embolism. The dashed and continuous lines are the projections of the frequency distribution of relative perfusion in the relative frequency *versus* perfusion control and relative frequency *versus* perfusion PE planes, respectively.

Discussion

The main finding of this study was that acute autologous blood clot PE increases ventilation in regions remaining perfused.

Animal Model and Global Physiologic Changes

The animal model of PE used in the study produced severe pulmonary embolization with obstruction of vessels carrying an average of 64% of the blood flow to the imaged areas during control conditions. This degree of obstruction is compatible with that of a previous study using autologous clots in dogs reaching similar pulmonary artery pressure targets.¹⁰

Despite the severe degree of embolization, no significant hypoxemia was observed in these sheep ventilated with $F_{IO_2} = 1.0$. Hypoxemia during PE has been reported to occur with \dot{V}_A/\dot{Q} mismatch¹¹ or preexisting right-to-left shunt such as a patent foramen ovale.¹² In our animal model there was no preexisting right-to-left shunt and use of $F_{IO_2} = 1.0$ eliminated any effect of increased \dot{V}_A/\dot{Q} mismatch. Thus, the absence of hypoxemia after PE indicates that no right-to-left shunt developed immediately after induction of embolism.

During clot injection, volume was administered in the form of crystalloids to correct hypotension. Thus, the observed increase in cardiac output with PE was probably a result of higher intravascular volume as expressed by the larger PAO pressure after PE. A possible mediator-dependent cardiovascular response following infusion of autologous clots^{13,14} could add to this change in cardiac output.

Increase in physiologic dead space is a major physiologic change observed during PE. It has been attributed to the contribution of high \dot{V}_A/\dot{Q} units from embolized regions.¹⁵ Delcroix *et al.*¹⁰ observed increases in inert gas-measured dead space with 10-mm emboli but a decrease when 1-mm emboli were used in an experimental dog model of PE with autologous blood clots. Significant collateral ventilation in dogs was the most probable explanation for these findings. In the current study, 7-mm emboli in sheep led to a marked increase in physiologic dead space and respiratory acidosis as the main respiratory physiopathological derangement, in line with the findings of Delcroix *et al.*¹⁰ for 10-mm emboli.

Positron Emission Tomography Technique

Several methods have been used to assess regional ventilation, such as inhaled microspheres, computed tomography, and topographical markers. Techniques that use aerosols, as the inhaled fluorescent microspheres method, may be limited by inertial and gravitational influences,¹⁶ presence of particles, deposition in the airway, and a distribution essentially dependent on con-

vection. Topographical markers can assess anatomic changes in regional volume but will not allow for characterization of the dynamics of gas exchange. The method used in this study to assess regional ventilation and perfusion represents a methodologic improvement as compared with these techniques. Because the tracer ¹³NN used is a gas, its regional distribution follows more closely that of other respiratory gases and not just the distribution of convective flow. Analysis of regional tracer distribution and washout with PET provides detailed assessment of local patterns of regional perfusion and ventilation. The obtained images of \dot{Q}_r allowed for topographical separation of the irregular areas of hypoperfusion and hyperperfusion after PE and investigation of their washout characteristics *in vivo*. Recently, a technique based on computed tomography and xenon washin was proposed to measure regional ventilation and perfusion.¹⁷ This technique may prove to be valuable to study regional gas exchange in similar settings.

The spatial resolution of our PET instrument of 6 mm is a limitation to the used technique. In addition, the range of the positrons, *i.e.*, the length positrons travel before annihilation in lung tissue, is estimated to be approximately 3 mm further degrading the resolution. This implies that any heterogeneity with length scales under this resolution will not be visualized.

The techniques used to quantify regional ventilation with injected ($s\dot{V}_{A,p}$) or inhaled ($s\dot{V}_{A,i}$) tracer measure related but distinct physiologic phenomena. Both assess a rate of gas transport out of a resolution element. $s\dot{V}_{A,p}$ is inherently limited to imaging ventilation of tracer initially present in perfused regions. Accordingly, it represents a perfusion-weighted mean $s\dot{V}_A$ of perfused alveoli within a ROI. Because it corresponds to alveoli that are perfused and ventilated, it is conceptually similar to the alveolar ventilation.

The $s\dot{V}_{A,i}$ characterizes the elimination of ¹³NN from all gas-filled areas within a ROI, including distal alveoli, unperfused alveoli, and serial dead space. Because inhaled ¹³NN content after equilibration is proportional to intraregional gas volume, $s\dot{V}_{A,i}$ represents a volume-weighted mean $s\dot{V}_A$. Thus, an explanation for the difference in results between $s\dot{V}_{A,p}$ and $s\dot{V}_{A,i}$ may be related to the effects of local dead space (stratified and alveolar) or to intraregional heterogeneity of local \dot{Q}_r and ventilation at length scales smaller than the spatial resolution of the PET camera or the ROI used to compute $s\dot{V}_{A,p}$ and $s\dot{V}_{A,i}$. In this line, local values of $s\dot{V}_{A,p}$ greater than those of $s\dot{V}_{A,i}$ would be evidence of an intraregional heterogeneity in $s\dot{V}_A$ distribution, which is closely correlated with intraregional \dot{Q}_r distribution. Conversely, $s\dot{V}_{A,p}$ less than $s\dot{V}_{A,i}$ could be taken as evidence of intraregional serial dead space being washed out at a faster rate than the more distal alveoli.

Regional Ventilation

Data from the literature on the magnitude and role of changes in regional ventilation during acute PE are unsettled. Regional pneumoconstriction induced by alveolar hypocapnia has been proposed as a mechanism to optimize \dot{V}_A/\dot{Q} matching. This phenomenon has been observed after unilateral PAO in dogs² and pigs¹ and indirectly suggested in a model of PE in dogs with clots 2–6 mm in diameter and 20–60 mm in length.⁷ Results from Simon *et al.*¹ during PAO indicate that the effect of lung hypoperfusion was related to changes in regional lung mechanics. The ratio of left-to-right lung impedance increased from 1.26 during control to 2.79 after left PAO.¹ Conversely, Altemeier *et al.*,¹⁸ using inhaled and injected microspheres, found minimal redistribution of ventilation with 780- μm beads in pigs. Tsang *et al.*¹⁹ studied dogs with microembolism induced with 250–1,000- μm polystyrene beads using a multibreath helium washout technique and did not find any significant changes in the heterogeneity of ventilation.

In the current study, a mean increase of 57% in $\dot{S}_{V_{A,P}}$ after severe PE was observed. Histograms of regional ventilation also indicated a change in ventilation distribution toward higher specific ventilations in perfused areas after embolism. Given that minute ventilation was kept constant, an increase in regional ventilation in perfused areas after PE must have corresponded to a concomitant decrease in \dot{S}_{V_A} in embolized areas. This would be consistent with the presence of higher residual tracer in areas with extreme reduction in \dot{Q} . Such inference was corroborated by measurements of inhaled tracer kinetics in three animals that showed specific ventilation to be increased in perfused areas and reduced in embolized areas after PE. Thus, we conclude that, in this model of PE, a change in regional specific ventilation occurs with PE, leading to slower washout rates in unperfused areas and increased washout rates of perfused regions. This phenomenon is compatible with the concept of hypocapnic pneumoconstriction described in other embolism and PAO models.^{1,2,7}

The magnitude of the changes in $\dot{S}_{V_{A,P}}$ within perfused regions after PE was larger than that for $\dot{S}_{V_{A,i}}$. As discussed in the section PET Technique, these measurements are not expected to lead to equal results. Previous studies in dogs showed that $\dot{S}_{V_{A,i}}$ and $\dot{S}_{V_{A,P}}$ had different distributions.^{8,20} We found that $\dot{S}_{V_{A,P}}$ tended to be larger and correlated with $\dot{S}_{V_{A,i}}$ in the perfused ROIs, and that these variables had a low correlation on a voxel-by-voxel basis. Such findings are in line with previous results.⁸

The $\dot{S}_{V_{A,P}}$ larger than $\dot{S}_{V_{A,i}}$ is evidence that, in those regions, regional ventilation matches regional perfusion better than regional volume.^{8,20} The common dead-space effect is an additional factor for the increased $\dot{S}_{V_{A,P}}$ after PE as studied in the Appendix.

The analysis of the washout curves after PE for the inhaled tracer experiments evidenced strong curvature

of the semilog washout plots. These curvilinear plots contrast with the mostly linear washout pattern during control conditions and demonstrate the development of significant intraregional ventilation heterogeneity after PE. The embolized areas presented the higher deviation from linearity. This may have resulted from intraregional heterogeneous bronchial or tissue mechanical properties^{1,5} leading to areas of either air trapping or very slow washout rate. The common dead-space effect could also generate a curvilinear washout (Appendix). However, this plays a minimal role in inhaled tracer measurements since ¹³NN is initially equilibrated in the whole lung. The perfused areas presented curvilinear washout plots that had smaller effect in the final washout of tracer than that of the embolized regions (fig. 4B). Several factors could be implicated: changes in intraregional mechanics due to release of intravascular mediators, partial overlapping of embolized and perfused regions, and the mentioned common dead-space effect.

Possible reasons for the differences between our results and those from previous studies may be related to several factors: different species, model of PE, and technique used to assess regional ventilation. Because hypocapnic pneumoconstriction is blunted even by low levels of inspired carbon dioxide,² homogenization of local concentrations of carbon dioxide is expected to reduce the pneumoconstrictive response. The anatomy of the distal airways and alveolar regions in different species provide for distinct degrees of distal gas mixing. Tsang *et al.*¹⁹ argued that significant collateral ventilation in dogs due to distal bronchoalveolar architecture with pores of Kohn, channels of Lambert, and channels of Martin could be responsible for homogenization of alveolar ventilation. This would contribute to rapid equilibration of carbon dioxide, reducing the possibility of regional hypocapnic pneumoconstriction during microembolization.

The particular model of PE used may be an important reason for distinct results. Autologous clots may produce regional release of active mediators that could modulate vascular and airway smooth muscle leading to different patterns of regional ventilation and perfusion distribution compared with inert emboli. Also, the size of the emboli used determines the size of embolized regions. In our model, embolism clearly affected large contiguous segments of the lungs with consequent large areas of hypocapnia. In contrast, during PE caused by microemboli, small embolized regions are interspersed between perfused regions. Homogenization of local alveolar carbon dioxide because of common dead space and intraregional mixing is more likely to occur in this case with blunting of the pneumoconstrictive response. In this line, large emboli, with large diffusive and convective pathways for gas mixing, are expected to produce greater regional hypoventilatory response unless other blunting mechanism was present. This proposition concurs with observations of a ventilatory shift re-

sponse to lung hypoperfusion in experiments with PAO in contrast to no shift observed with microembolism. Our results extend these observations to the setting of autologous blood clot pulmonary macroembolism. We showed that also in the situation of an irregular pattern of vascular obstruction as opposed to occlusion of a major branch of the pulmonary artery, a redistribution of regional ventilation is observed with a shift toward perfused areas.

Another factor could be the sensitivity of the technique to detect changes in regional ventilation at small length scales. As stated previously, techniques that use aerosol particles to track ventilation are affected by inertial and gravitational influences,¹⁶ clustering of particles, deposition in large airway walls, and a distribution exclusively dependent on convection. The technique used in the current study is based on kinetic behavior of ¹³NN, a gas that undergoes diffusive and convective transport as other respired gases. Thus, injecting this gas intravenously and following its transport from the pulmonary vasculature to the alveoli and its subsequent ventilatory elimination should represent more accurately the regional transport of respiratory gases.

Substantial systemic acidosis and hypercapnia were present after embolization in our series of experiments. It could be speculated that these also influence the pneumoconstrictive response. Consistent with this hypothesis was the finding that the increase in washout rate from perfused areas caused by PE was correlated with the systemic blood pH after embolism. The greater the degree of acidosis, the lesser the redistribution of $\dot{V}_{A,P}$ toward perfused regions. More research is needed to characterize the modulation of the regional ventilatory response to PE by the acid-base state.

Despite the substantial (approximately 50%) ventilatory increase in perfused regions, its extent was not entirely equivalent to the changes in \dot{Q}_r created by PE, and thus it was not enough to preserve \dot{V}_A/\dot{Q} matching (fig. 1). Increases in \dot{V}_A/\dot{Q} heterogeneity during PE have been previously reported.^{11,21} The magnitude of the regional response necessary to produce the average 57% increase in ventilation of perfused images in our experiments can be roughly estimated if it is considered that: (1) total minute ventilation was not changed during the experiment; (2) before PE, specific ventilation was equal in regions that became perfused or embolized after PE; and (3) the regional volume of embolized regions was approximately 65% of the total lung volume. In this case, it can be shown that the ratio of specific ventilations of perfused to embolized regions would approximate 2.2. Thus, our study suggests that, in this model of acute PE with autologous blood clots, PE elicits a change in regional specific ventilation in embolized and perfused areas from initially equal values to values differing by approximately

100%. Such redistribution of specific regional ventilation improves \dot{V}_A/\dot{Q} matching after severe PE.

Spatial Correlation of Ventilation and Perfusion Data.

Previous work from our group for a single-slice PET camera in dogs revealed significant correlation of regional volume and regional ventilation with perfusion while in the prone position.⁸ Our results in the control condition confirm such observations in prone sheep in the used multiring PET camera.

As expected, the spatial correlation between regional perfusion before and after PE was very low given the severity of the pulmonary vasculature obstruction in our model. With this degree of obstruction of the pulmonary vessels, areas of both high and low perfusion before PE were obstructed after PE. One could have expected that regions of higher perfusion could have received the majority of the emboli. However, given the incremental mode of injection of the emboli during up to 1 h, areas of initial low flow could have become areas of increased flow after obstruction of other pulmonary vessels.

High degree of spatial correlation between perfusion and gas volume at control conditions represents higher blood flow to areas of greater gas content. A decrease of this correlation was observed after PE in the regions that remained perfused. Given that V_r changed less than \dot{Q}_r , the reduction in the spatial correlation between \dot{Q}_r and V_r reflects primarily the increased heterogeneity in the distribution of perfusion caused by vascular obstruction.

Spatial correlation of $\dot{V}_{A,P}$ with \dot{Q}_r also tended to decrease after PE. This reduction was observed despite the demonstrated increase in regional specific ventilation of perfused areas. Such finding reveals the incomplete capacity of regional controlling mechanisms of ventilation distribution to compensate for the severe heterogeneity of perfusion distribution induced in this model of PE. The degree of compensation when less dramatic changes are present is not apparent from this study and deserves further investigation. It is conceivable that in situations of less severe changes, less blunting of compensatory mechanisms would occur and higher spatial correlation between local ventilation and perfusion would be maintained.

Modeling of Contribution of Embolized Areas to Tracer Washout

An alternative mechanism for the increased washout of injected tracer from perfused regions after PE is the common dead-space effect. Tracer-free gas from embolized regions would mix through the common dead space with tracer-containing gas originated from perfused areas. This mechanism would result in effective dilution of the ¹³NN tracer in the perfused areas along the washout without changes in tidal ventilation of these areas. The

mechanism has been examined previously as related to gas exchange and steady state PET measurements.^{22,23}

To evaluate the effect of mixing by a common dead space, we simulated the washout of a tracer with compartment models (Appendix). The models were chosen to evaluate the effect of a common dead space at a regional or global level. They are not an anatomic description of the lungs but a theoretical formulation that allows for the evaluation of the expected regional and global dead space on ¹³NN gas kinetics. The simulations indicated that, even in the absence of changes in regional bulk flow, an increase in regional washout of tracer containing areas could be observed. However, the magnitude of this effect is significantly smaller than that observed in our experiments, suggesting that additional redistribution of regional ventilation had to be present to explain the measured changes in $\dot{V}_{A,P}$.

In summary, we showed that an increase in regional specific ventilation to perfused regions occurs after severe PE with cylindrical 7-mm diameter by 7-mm length autologous clots in mechanically ventilated, anesthetized sheep. This increase in local ventilation leads to improved gas exchange as compared with an otherwise unchanged ventilation distribution by improving matching of ventilation to perfusion.

The authors thank Steven B. Weise (Senior Research Technologist, PET Imaging Laboratory, Massachusetts General Hospital) for his expert support in the acquisition of images.

References

- Simon BA, Tsuzaki K, Venegas JG: Changes in regional lung mechanics and ventilation distribution after unilateral pulmonary artery occlusion. *J Appl Physiol* 1997; 82:882-91
- Severinghaus JW, Swenson EW, Finley TN, Lategola MT, Williams J: Unilateral hypoventilation produced in dogs by occluding one pulmonary artery. *J Appl Physiol* 1961; 16:53-60
- Moore RL, Humphreys GH, Cochran HW: The effect of sudden occlusion of either primary pulmonary artery on cardiac output and pulmonary expansion. *J Thorac Surg* 1934; 3:573-89
- Ingram RH Jr: Effects of airway versus arterial CO₂ changes on lung mechanics in dogs. *J Appl Physiol* 1975; 38:603-7
- Oldmixon EH, Carlsson K, Kuhn C 3rd, Butler JP, Hoppin FG Jr: Alpha-Actin: Disposition, quantities, and estimated effects on lung recoil and compliance. *J Appl Physiol* 2001; 91:459-73
- Thomas DP, Stein M, Tonabe G: Mechanism of bronchoconstriction produced by thromboemboli in dogs. *Am J Physiol* 1964; 206:1207-12
- Levy SE, Simmons DH: Redistribution of alveolar ventilation following pulmonary thromboembolism in the dog. *J Appl Physiol* 1974; 36:60-8
- Treppo S, Mijailovich SM, Venegas JG: Contributions of pulmonary perfusion and ventilation to heterogeneity in $V(A)/Q$ measured by PET. *J Appl Physiol* 1997; 82:1163-76
- Mijailovich SM, Treppo S, Venegas JG: Effects of lung motion and tracer kinetics corrections on PET imaging of pulmonary function. *J Appl Physiol* 1997; 82:1154-62
- Delcroix M, Melot C, Vanderhoeft P, Naeije R: Embolus size affects gas exchange in canine autologous blood clot pulmonary embolism. *J Appl Physiol* 1993; 74:1140-8
- Santolucando A, Prediletto R, Fornai E, Formichi B, Begliomini E, Giannella-Neto A, Giuntini C: Mechanisms of hypoxemia and hypocapnia in pulmonary embolism. *Am J Respir Crit Care Med* 1995; 152:336-47
- Kasper W, Geibel A, Tiede N, Just H: Patent foramen ovale in patients with haemodynamically significant pulmonary embolism. *Lancet* 1992; 340:561-4
- Taheri SA, Shenoy S, Murawski S, Divan K, Cullin J, Mousa S: Diagnosis of pulmonary embolism by use of urinary TNF alpha and its soluble TNF receptor I. *Angiology* 1999; 50:703-6
- Breuer J, Meschig R, Breuer HW, Arnold G: Effects of serotonin on the cardiopulmonary circulatory system with and without 5-HT₂-receptor blockade by ketanserin. *J Cardiovasc Pharmacol* 1985; 7:S64-6
- Elliott CG: Pulmonary physiology during pulmonary embolism. *Chest* 1992; 101:1635-71S
- Darquenne C, Paiva M: Two- and three-dimensional simulations of aerosol transport and deposition in alveolar zone of human lung. *J Appl Physiol* 1996; 80:1401-14
- Kreck TC, Krueger MA, Altemeier WA, Sinclair SE, Robertson HT, Shade ED, Hildebrandt J, Lamm WJ, Frazer DA, Polissar NL, Hlastala MP: Determination of regional ventilation and perfusion in the lung using xenon and computed tomography. *J Appl Physiol* 2001; 91:1741-9
- Altemeier WA, Robertson HT, McKinney S, Glenn RW: Pulmonary embolization causes hypoxemia by redistributing regional blood flow without changing ventilation. *J Appl Physiol* 1998; 85:2337-43
- Tsang JY, Frazer D, Hlastala MP: Ventilation heterogeneity does not change following pulmonary microembolism. *J Appl Physiol* 2000; 88:705-12
- Venegas JG: Noninvasive measurement of local VA, Q and VA/Q distributions by PET, Complexity in Structure and Function of the Lung, 1st edition. Edited by Hlastala MP, Robertson HT. New York, Marcel Dekker, 1998, pp 483-510
- Manier G, Castaing Y, Guenard H: Determinants of hypoxemia during the acute phase of pulmonary embolism in humans. *Am Rev Respir Dis* 1985; 132:332-8
- Rhodes CG, Valind SO, Brudin LH, Wollmer PE, Jones T, Hughes JM: Quantification of regional V/Q ratios in humans by use of PET: I. Theory. *J Appl Physiol* 1989; 66:1896-904
- Ross BB, Farhi LE: Dead-space ventilation as a determinant in the ventilation-perfusion concept. *J Appl Physiol* 1960; 15:363-71
- Stahl WR: Scaling of respiratory variables in mammals. *J Appl Physiol* 1967; 22:453-60

Appendix

Modeling the Contribution of Embolized Areas to Tracer Washout: Effect of Parallel Dead Space

We used two simple models of ventilation washout to evaluate the contribution of embolized areas to the washout of injected tracer: a two-compartment model and a four-compartment model distributed as two groups of two regions (fig. 7).

The two-compartment model was conceptualized as two units, A and B, representing the perfused and embolized areas after PE, respectively (fig. 7A). These regions were connected to a common dead space (V_D). Washout of a tracer from these regions was described as:

$$F_A(i) = \frac{F_A(i-1) \cdot V_A + F_D(i-1) \cdot V_D \cdot f_v}{V_A + f_v \cdot (V_D + V'_A)} \quad (A1)$$

$$F_B(i) = \frac{F_B(i-1) \cdot V_B + F_D(i-1) \cdot V_D \cdot (1 - f_v)}{V_B + (1 - f_v) \cdot (V_D + V'_A)} \quad (A2)$$

where $F_x(i)$ = fraction of tracer in compartment x (A or B) at end of breath i, V_A = volume of compartment A at end expiration, V_B = volume of compartment B at end expiration, V_D = volume of common dead space, f_v = fraction of ventilation received by compartment A, and V'_A = portion of inspired volume free of tracer gas.

The four-compartment model was used to study the effect of dividing the total serial dead space into a regional and a global common dead space (fig. 7B). The model was devised as two regions, A and B, with a common dead space (V_D). Each region contained two compartments (A1, A2, and B1, B2) with local dead space V_{DA} and V_{DB} . Compartment A1 represented the perfused regions after PE, i.e., regions filled with tracer gas at the beginning of the washout. Compartment A2 represented the embolized areas within the same region of A1, thus with same regional and common dead space. Compartments B1 and B2 were embolized areas sharing the same common dead space (V_D). Embolized areas were simulated as tracer free at the beginning of the washout. Total functional residual capacity (FRC) and inspired dead-space volumes were distributed to the compartments assuming that a fraction α was assigned to compartment A1 and a fraction $(1 - \alpha)/3$ was assigned to A2, B1, and B2.

The following equations describe the washout of a tracer from each compartment:

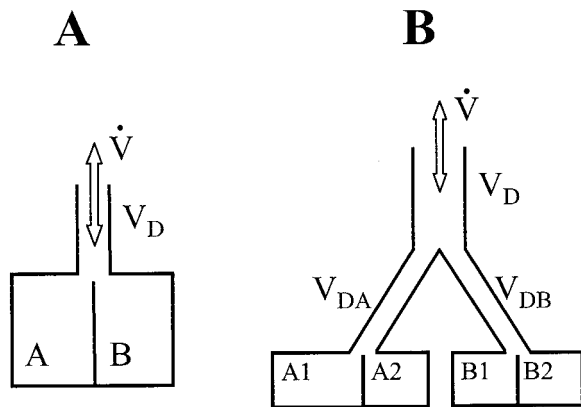


Fig. 7. Compartment models for analysis of dead-space effect in tracer washout. (A) Two-compartment model: A represents the tracer-containing perfused region and B the tracer-free embolized region at the beginning of the washout. (B) Four-compartment model: A1 represents the perfused compartment that receives tracer and A2, B1, and B2 the tracer-free embolized regions. \dot{V} = minute ventilation; V_D = volume of common dead space; V_{DA} = volume of regional dead space for compartments A1 and A2; V_{DB} = volume of regional dead space for compartments B1 and B2.

$$F_{A1}(i) = \frac{F_{A1}(i-1) \cdot V_{A1} + F_D(i-1) \cdot V_D \cdot \alpha + F_{DA}(i-1) \cdot V_{DA} \cdot \alpha}{V_{A1} + \alpha \cdot (V_D + V_{DA} + V'_A)} \quad (A3)$$

$$F_{A2}(i) = \frac{F_{A2}(i-1) \cdot V_{A2} + F_D(i-1) \cdot V_D \cdot (1-\alpha)/3 + F_{DA}(i-1) \cdot V_{DA} \cdot (1-\alpha)/3}{V_{A2} + (V_D + V_{DA} + V'_A) \cdot (1-\alpha)/3} \quad (A4)$$

$$F_{B1}(i) = F_{B2}(i) = \frac{F_{B1}(i-1) \cdot V_{B1} + F_D(i-1) \cdot V_D \cdot (1-\alpha)/3 + F_{DB}(i-1) \cdot V_{DB} \cdot (1-\alpha)/3}{V_{B1} + (V_D + V_{DA} + V'_A) \cdot (1-\alpha)/3} \quad (A5)$$

$$F_{VD}(i) = F_{A1}(i) \cdot \alpha + (F_{A2}(i) + 2 \cdot F_{B1}(i)) \cdot (1-\alpha)/3 \quad (A6)$$

$$F_{VDA}(i) = \frac{F_{A1}(i) \cdot \alpha + F_{A2}(i) \cdot (1-\alpha)/3}{(\alpha + (1-\alpha)/3)} \quad (A7)$$

$$F_{VDB}(i) = F_{B1}(i) \quad (A8)$$

where $F_x(i)$ = fraction of tracer in compartment x at end of breath i, V_D = volume of common dead space, V_{DA} = volume of regional dead space for compartments A1 and A2, V_{DB} = volume of regional dead-space for compartments B1 and B2, V_{A1} = volume of compartment A1 at end expiration = $\alpha \cdot \text{FRC}$, $V_{A2} = V_{B1} = V_{B2}$ = volume of the respective compartments A2, B1, and B2 at end expiration = $(1-\alpha)/3 \cdot \text{FRC}$, and V'_A = portion of the inspired volume free of tracer. If V_T = inspired volume, $V'_A = V_T - (V_D + V_{DA} + V_{DB})$; α = fraction of perfused region.

Input data for the model was derived from tidal volumes and respiratory rates used during the experiments, and sheep dead space was estimated from previous regression equations.²⁴ Simulations assumed a respiratory rate of 12 breaths/min and FRC = 1,000 ml. The following

Table 2. Conditions Studied in the Simulations of Tracer Washout with the Two- and Four-compartment Models and Derived Specific Ventilation of the Tracer-containing Compartment (A or A1) Computed from the Three First Points of the Washout Curve

Condition	f_v	V_D (ml)	V_{DA} (ml)	V_T (ml)	F_{Bo}	$s\dot{V}_A$ (s)
2-C homogeneous \dot{V}/V , equal initial concentration	0.35	50	—	250	1	0.0158
2-C homogeneous \dot{V}/V	0.35	50	—	250	0	0.0187
4-C homogeneous \dot{V}/V	0.35	30	10	250	0	0.0174
2-C homogeneous \dot{V}/V small V_D	0.35	5	—	205	0	0.0161
2-C heterogeneous \dot{V}/V	0.55	50	—	250	0	0.0262

f_v = fraction of ventilation to compartment A or A1; V_D = volume of common dead space; $V_{DA} = V_{DB}$ = volume of regional dead space; V_T = tidal volume; F_{Bo} = initial concentrations in compartment B and A2; $s\dot{V}_A$ = derived specific ventilation; 2-C = two-compartment model; \dot{V}/V = ventilation/volume; 4-C = four-compartment model; α = fraction of FRC to compartment A or A1 = 0.35; F_{Ao} and F_{A1o} = initial concentrations in compartments A and A1 = 1.

effects were studied using the values presented in table 2: (1) parallel dead-space ($F_{Bo} = 0$) with homogeneous ventilation/volume distribution; (2) parallel dead space ($F_{A2} = 0$ and $F_{Bo} = 0$) with division of the total serial dead space into a regional and a global common dead space; (3) reduction of the common dead space with parallel dead space and homogeneous ventilation/volume distribution; and (4) heterogeneous ventilation/volume distribution with increased ventilation toward the tracer-containing areas. $s\dot{V}_A$ computed from each of these conditions could be compared with the situation of homogeneous ventilation/volume distribution and equal initial concentration of tracer in regions A and B (table 2).

The simulations indicated that presence of a tracer-free area in parallel with a tracer-containing region promoted an increased washout of the tracer-containing region (table 2). The specific ventilation of compartment A ($s\dot{V}_A$) increased by 18% because of the presence of the tracer-free region B. Partition of the total dead space into a global common dead space and regional dead spaces had the effect of reducing that value from 18 to 10% as compared with a global dead space with the same volume of the added regional and global V_{Ds} . Superimposition of a ventilation/volume heterogeneity increasing ventilation to the tracer containing area by 57% increased $s\dot{V}_A$ from 0.0158 to 0.0262 (66%). Reduction of the common dead space (V_D) with consequent reduced mixing of the parallel compartments reduced $s\dot{V}_A$. The total effect measured in our experimental washout curves (average increase in $s\dot{V}_{A,p}$ of 57%) was more than three times larger than the largest effect obtained in these simulations for the exclusive effect of a parallel dead space ($F_{Bo} = 0$). It would be expected that in the experiments larger regional dead-space effect would be present, and thus the maximum effect of a parallel dead space would be smaller than the 18% increase in $s\dot{V}_{A,p}$. As expected, significant increase in the washout rate during the simulations was observed when an increase in specific ventilation was introduced in the tracer containing regions. Such results suggest that additional factors (increased regional ventilation of perfused areas after PE caused by impedance changes in embolized areas) should be present to explain the observed increase of regional specific ventilation in areas remaining perfused after PE.